Journal of Nuclear Materials 376 (2008) 240–246

Contents lists available at ScienceDirect

Journal of Nuclear Materials

journal homepage: www.elsevier.com/locate/jnucmat

Deformation and fracture properties in neutron irradiated pure Mo and Mo alloys

T.S. Byun [a,*], M. Li [a], B.V. Cockeram [b], L.L. Snead [a]

[a] Oak Ridge National Laboratory, P.O. Box 2008, Oak Ridge, TN 37831, USA
[b] Bechtel-Bettis, Inc., P.O. Box 79, West Mifflin, PA 15122-0079, USA

ARTICLE INFO

Article history:
Received 3 January 2008
Accepted 5 March 2008

ABSTRACT

The effect of neutron irradiation on the mechanical properties of select molybdenum materials, unalloyed low carbon arc-cast (LCAC) Mo, Mo–0.5% Ti–0.1% Zr (TZM) alloy, and oxide dispersion-strengthened (ODS) Mo alloy, was characterized by analyzing the temperature dependence of mechanical properties. This study assembles the tensile test data obtained through multiple irradiation and post-irradiation experiments, in which tensile specimens were irradiated up to 13.1 dpa at 80–1000 °C and tested at −194 to 1000 °C. Irradiation at 80–609 °C increased yield stress significantly, up to 170%, while the increase of yield stress after irradiation at 784–936 °C was not significant. The plastic instability stress was strongly dependent on test temperature but was nearly independent of irradiation dose and temperature. The true fracture stress showed weak dependences on test temperature, irradiation dose and temperature when ductile failure occurred. Among the test materials the stress-relieved ODS material in the longitudinal direction (ODS-LSR) displayed the highest resistance to irradiation embrittlement due to its relatively high fracture stress. The critical temperature for shear failure (CTSF) was defined and evaluated for the test materials and the CTSF values were compared with the ductile-to-brittle transition temperatures (DBTT) based on ductility data.

Published by Elsevier B.V.

1. Introduction

Molybdenum and its alloys have been candidate structural materials for high-temperature applications because of their outstanding heat-conducting capabilities and high-temperature strength [1–7]. The molybdenum materials are also considered as candidate materials for fusion reactor components such as plasma facing components (PFC) and diverter components because of their relatively low sputtering yield, high thermal conductivity, and good thermal compatibility with other component materials such as copper alloys and steels [8–12]. Moreover, molybdenum is often used as a surrogate for understanding the effects of irradiation and materials properties of tungsten, which is another PFC material. In displacive radiation environments, however, the low ductility and radiation induced embrittlement observed in these materials have been a main concern [1–13].

Since polycrystalline molybdenum can inherently weak grain boundaries, grain boundary strengthening and refinement techniques have been used to prevent or delay grain boundary embrittlement [13–25]. Significant improvement in ductility and fracture toughness has been achieved so far mainly by controlling impurities, reducing the grain size, and adding alloy elements such as Re, Ti, Zr, Al, B, and C, or oxide and carbide particles. Three molybdenum materials: low carbon arc-cast (LCAC) Mo, Mo–0.5% Ti–0.1% Zr (TZM) alloy, and oxide dispersion-strengthened (ODS) Mo alloy, have been studied for nuclear applications. The LCAC Mo is unalloyed molybdenum with low levels of impurities (∼tens of ppm of oxygen and a few ppm of nitrogen) and a controlled amount of carbon (⩽100 ppm) added for grain boundary strengthening [4–6,19,26–28]. This metal has outstanding strength over a wide temperature range and good ductility at ambient temperature, and is a reference material for comparison in this paper. Molybdenum's most commonly used alloy is TZM, which is micro-alloyed molybdenum with small amounts of titanium, zirconium, and carbon for precipitation strengthening by titanium and zirconium carbides as well as for solid solution hardening [3,5,8–10,15–17,19]. The TZM alloy retains high strength at temperatures over 1000 °C, often more than twice the strength of pure molybdenum, and its recrystallization temperature is also higher than that of pure molybdenum. The third molybdenum material, ODS Mo (or Mo–La), is a fine grained molybdenum doped with lanthanum oxide particles [3,7]. This material has extraordinary resistance to recrystallization and high-temperature deformation, and therefore, is suitable for applications requiring high strength at high-temperatures.

This paper provides a comparison of mechanical property parameters for the three molybdenum materials before and after irradiation that have been determined from data previously reported in the literature [3–7,27–29]. Also, the comparison is intended to more clearly reveal the characteristic mechanical behaviors of each molybdenum material. Temperature dependences in

* Corresponding author. Tel.: +1 865 576 7738.
E-mail address: byunts@ornl.gov (T.S. Byun).

0022-3115/$ - see front matter Published by Elsevier B.V.
doi:10.1016/j.jnucmat.2008.03.004

yield stress, plastic instability stress, and true fracture stress were compared for the irradiated and nonirradiated materials in stress-relieved condition (for the three materials) and recrystallized condition (for LCAC Mo only).

2. Experiment and analysis method

2.1. Irradiation and tensile testing

Since the experimental details regarding molybdenum materials and neutron irradiations have been described in previous publications [3–7,27–29], only a summarized description of the experiments is provided below. The test materials, low carbon arc-cast (LCAC) Mo, Mo–0.5% Ti–0.1% Zr (TZM) alloy, and oxide dispersion-strengthened (ODS) Mo alloy, were obtained from H.C. Starck, Inc, in the form of wrought sheets or plates with thicknesses of 0.508 mm, 6.35 mm, and 0.76 mm, respectively. The chemical compositions of the molybdenum alloys reported by the manufacturer are listed in Table 1. The final heat treatment following wrought processes was stress-relief anneal in vacuum at 850 °C (or 900 °C) for 1 h, 1150 °C for 1 h (or 0.5 h), and 1200 °C for 1 h for LCAC, TZM, and ODS Mo, respectively. Also, the final heat treatment for some wrought LCAC Mo specimens was recrystallization at 1200 °C for 1 h.

Sub-sized SS-1 and SS-3 type specimens, with gage section dimensions of $20.32 \times 0.52 \times 0.4$–$0.76$ mm and $7.62 \times 1.52 \times 0.76$ mm, respectively, were used for the tensile testing. The wrought and heat-treated sheets and plates were machined into these geometries and electrochemically cleaned before irradiation. Specimens were loaded into aluminum rabbit capsules for irradiations at ~300 °C and vanadium capsules for higher temperature irradiations. These non-perforated, helium-filled capsules were irradiated in the peripheral target positions (PTP) of the High Flux Isotope Reactor (HFIR) at Oak Ridge National Laboratory. Irradiation temperature was controlled by the gas gaps in these non-perforated capsules. Irradiation temperatures were determined within ±20 °C by use of the electrical resistivity technique for a passive SiC temperature monitor. The perforated aluminum rabbit capsules allowing contact with the flowing coolant in the hydraulic tube (HT) were used for part of the LCAC Mo specimens (LCAC-LR) to maintain the specimen temperature at ~80 °C. Table 2 lists materials and irradiation conditions.

As listed in Table 2, irradiation experiments have been performed in different series of rabbit capsules: N1–N4, K1–K2, F1–F6, and KP1–KP7. The N and K-series capsules were used for irradiations of LCAC Mo in LR, LSR, and TSR conditions and of TZM and ODS Mo in LSR and TSR conditions to 1.2–3.9 dpa at 560–936 °C. All three materials in LSR conditions were irradiated in F1–F6 capsules in a similar temperature range to higher dose, 12.3–13.1 dpa. The perforated KP1–KP7 capsules were used in the low-temperature (~80 °C) irradiation for LCAC Mo in LR condition and contained SS-3 specimens. Doses for these SS-3 specimens were in the range of 0.00072–0.28 dpa. Note that both fluence and dpa are given for each capsule in Table 2, and they have a linear relationship dpa $\approx 0.0531 \times f$, where f is the fast neutron fluence ($E > 0.1$ MeV) $\times 10^{-24}$ n/m^2.

Tensile tests were preformed in a vacuum of $\sim 10^{-4}$ Pa at a nominal strain rate of 10^{-3} s^{-1} at temperatures ranging from −100 to 300 °C for SS-3 specimens (or LCAC-LR specimens) and from −194 to 1400 °C for SS-1 specimens (the maximum test tempera-

Table 2
Materials, capsules irradiated in HFIR, and irradiation conditions

Material	Heat treatment and direction	Capsule	Irr. temp. (°C)	Fluence × 10^{24} n/m^2 ($E > 0.1$ MeV)	Dose (dpa)	Specimen type [reference]
LCAC	LR	KP1	80	0.002	0.000072	SS-3 [27–29]
LCAC	LR	KP2	80	0.02	0.00072	SS-3 [27–29]
LCAC	LR	KP3	80	0.2	0.0072	SS-3 [27–29]
LCAC	LR	KP4	80	2	0.072	SS-3 [27–29]
LCAC	LR	KP5	80	7.88	0.28	SS-3 [27–29]
LCAC	LR	KP6	80	0.81	0.029	SS-3 [27–29]
LCAC	LR	KP7	80	0.084	0.003	SS-3 [27–29]
LCAC	LSR	F1	294	232	12.3	SS-1 [5,7]
LCAC	LSR	F2	294	232	12.3	SS-1 [5,7]
LCAC	LSR	F3	784	246	13.1	SS-1 [5,7]
LCAC	LSR	F4	560	246	13.1	SS-1 [5,7]
LCAC	LSR	F5	936	247	13.1	SS-1 [5,7]
LCAC	LSR	F6	936	247	13.1	SS-1 [5,7]
LCAC	LSR	KP6	80	0.81	0.029	SS-3 [27–29]
LCAC	LSR	KP7	80	0.084	0.003	SS-3 [27–29]
ODS	LSR	F1	294	232	12.3	SS-1 [7]
ODS	LSR	F2	294	232	12.3	SS-1 [7]
ODS	LSR	F3	784	246	13.1	SS-1 [7]
ODS	LSR	F4	560	246	13.1	SS-1 [7]
ODS	LSR	F5	936	247	13.1	SS-1 [7]
ODS	LSR	F6	936	247	13.1	SS-1 [7]
ODS	LSR	K1	870	22.8	1.2	SS-1 [7]
ODS	LSR	K2	870	64.4	3.4	SS-1 [7]
ODS	LSR	N1	609	72.6	3.9	SS-1 [6,7]
ODS	TSR	K1	870	22.8	1.2	SS-1 [6,7]
ODS	TSR	K2	870	64.4	3.4	SS-1 [6,7]
ODS	TSR	N1	609	72.6	3.9	SS-1 [6,7]
TZM	LSR	F1	294	232	12.3	SS-1 [5]
TZM	LSR	F2	294	232	12.3	SS-1 [5]
TZM	LSR	F3	784	246	13.1	SS-1 [5]
TZM	LSR	F4	560	246	13.1	SS-1 [5]
TZM	LSR	F5	936	247	13.1	SS-1 [5]
TZM	LSR	F6	936	247	13.1	SS-1 [5]
TZM	LSR	N2	560	72.6	3.9	SS-1 [5]
TZM	LSR	N4	936	73.3	3.9	SS-1 [5]
TZM	TSR	N2	560	72.6	3.9	SS-1 [5]
TZM	TSR	N4	936	73.3	3.9	SS-1 [5]

Note: LSR – longitudinal, stress-relieved; TSR – transverse, stress-relieved; LR – longitudinal, recrystallized.

Table 1
Chemical compositions of LCAC, TZM, and ODS alloys and their specimen directions and final heat treatments

Material	Chemical compositions (in wppm)										Heat treatment/specimen direction
	C	O	N	Ti	Zr	Fe	Ni	Si	La	Al, Cu, Ca, Cr, Mg, Pb, Sn	
LCAC	90	3	4			10	<10	<10			LSR
											TSR
											LR
LCAC*	140	6	8								LR
TZM	223	17	9	5000	1140	<10	<10	<10			LSR
											TSR
ODS	40			<10		27	<10	<10	10800	<10	LSR
											TSR

Note: LSR – longitudinal, stress-relieved; TSR – transverse, stress-relieved; LR – longitudinal, recrystallized. LCAC* - material only for SS-3 specimens.

ture for irradiated was 1000 °C). True stress parameters such as yield stress (YS), plastic instability stress (PIS), and true fracture stress (FS) were obtained from load–displacement records.

2.2. Calculation of true stress parameters

The calculation procedure for the above stress parameters is briefly described here since the details and backgrounds are given elsewhere [30–32]. YS was obtained from upper yield load (or 0.2% yield load for continuous yielding) divided by the initial cross sectional area of specimen. The PIS is defined as the true stress version of the engineering ultimate tensile strength (UTS), where the onset of plastic instability (necking) occurs, and is calculated from tensile test data, UTS and uniform plastic strain ε_U^P, using a constant volume condition for plastic deformation [30]:

$$\mathrm{PIS} = \mathrm{UTS} \times \exp(\varepsilon_U^P). \quad (1)$$

Unless the specimen breaks in a fully brittle mode, a linear hardening approximation during necking and iterative calculation method were used to obtain the true fracture stress, FS, from either of measured engineering fracture stress or reduction of area. In modeling a constitutive equation for unstable deformation, it is considered that the true stress–true strain curve starts from the higher one of YS or PIS, and the YS can be higher than the PIS after irradiation and that the true stress in the tensile direction is approximately linear to the true strain. This leads to the following linear true stress–true strain relationship with necking strain [31,32]:

$$\mathrm{FS} = \max(\mathrm{YS}, \mathrm{PIS}) + \mathrm{PIS} \times (\varepsilon_F^P - \varepsilon_U^P), \quad (2)$$

where ε_U^P and ε_F^P are the true uniform plastic strain, and the plastic strain at fracture, respectively. Also, FS can be calculated from the engineering fracture stress (EFS) using the constant volume condition:

$$\mathrm{FS} = \mathrm{EFS} \times \exp(\varepsilon_F^P). \quad (3)$$

The solution for ε_F^P and FS can be obtained by iterative calculations using these two equations. The following discussion focuses on temperature dependence and irradiation effects in these true stress and strain parameters.

3. Results and discussion

3.1. Yield stress and irradiation hardening

It is known that neutron irradiation of molybdenum at temperatures below ~700 °C can result in a significant increase of strength and loss of ductility [1,4–6,27–33]. For this reason, the temperature dependence of yield stress is displayed separately for the irradiation temperatures lower and higher than 700 °C. Fig. 1(a) and (b) compare the yield stresses after low-temperature (<700 °C) and high-temperature (>700 °C) irradiations, respectively, with the same baseline data from nonirradiated materials. For some irradiated materials, fracture stress was measured at temperatures below the DBTT as brittle failure mode occurred and no plasticity was exhibited. In such cases the fracture stress values were used for yield stress values. The yield stress of the nonirradiated materials monotonically decreases with temperature above about −100 °C, below which some specimens show reduced yield stress (or fracture stress) due to brittle failure. It is seen that the decreasing rate is high at relatively low-temperatures <~200 °C and becomes much lower at intermediate temperatures. The yield stress drops again at ~1000 °C where a creep mechanism is believed to operate. It is noticed that the TZM alloy has the highest yield stress at elevated temperatures; which becomes more apparent at ~1000 °C and above. The 1200 °C annealed LCAC-LR material has significantly lower yield stress than others due to the larger grain size [4].

In the study all stress-relieved materials were irradiated to at least 1.2 dpa and it is believed that the radiation effects on microstructure and strength have almost saturated at this dose level [27,30]. As seen in Fig. 1(a), irradiation hardening is significant only after irradiations at relatively low-temperatures ⩽609 °C. The highest irradiation hardening is found in the ODS Mo, which displays up to 2.7 times higher yield (or fracture) stress after irradiation to 13.2 dpa at 294 °C. The LCAC-LR material irradiated to 0.072–0.28 dpa shows similar percent increase of yield stress as the other materials in stress-relieved condition. Fig. 1(b) indicates that irradiation at higher temperatures (>700 °C) does not induce a significant increase in yield stress. Measurable irradiation hardening is found only in ODS Mo specimens tested below room-temperature and in a few TZM Mo specimens tested at 600 and 700 °C.

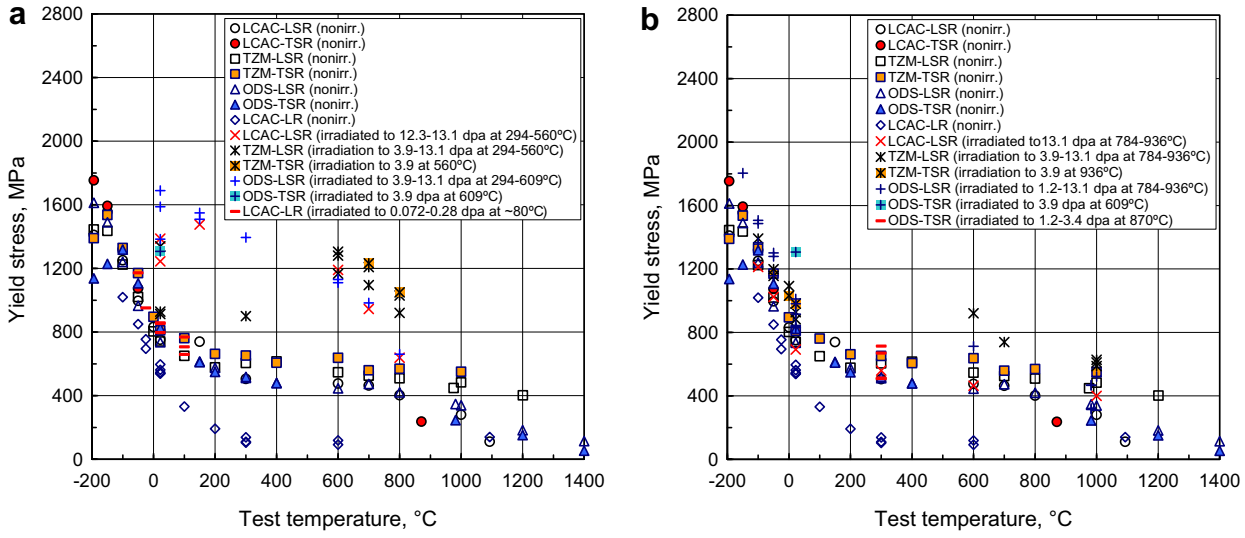

Fig. 1. Temperature dependence of yield stress before irradiation in (a) and (b) and after irradiation (a) at relatively low-temperatures (<700 °C) and (b) at high temperatures (>700 °C).

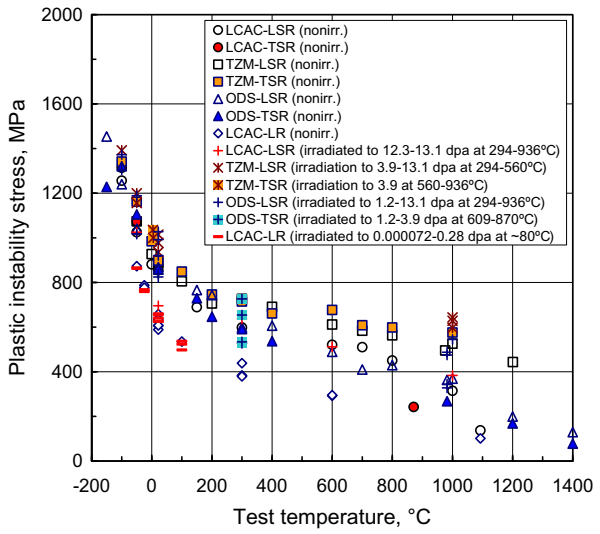

Fig. 2. Temperature dependence of plastic instability stress before and after irradiation.

The difference in irradiation hardening between the temperature ranges, below and above ~700 °C, can be explained by the difference in the mobility of point defects in those temperature ranges [4–6,32–37]. Irradiation hardening usually results from the formation of numerous fine point defect clusters, dislocation loops, or voids, depending on irradiation temperature. During irradiation at relatively low-temperatures the annihilation of these defect clusters is slow because of the low mobility of point defects to sinks. At higher irradiation temperatures such thermally activated annihilation or recovery of properties occurs at a faster rate by different mechanisms [6,35]. The annihilation behavior of such defect clusters has been measured by microhardness, positron annihilation, or electrical resistivity techniques [6,38]. Recently, the hardness and electrical resistivity of the LCAC molybdenum were measured after irradiation at 270–1100 °C and neutron fluences of 10.5–64.4 $\times$ 10^{24} n/m^2 (E > 0.1 MeV) [6]. In isochronous annealing the recovery of radiation hardening in the specimens irradiated at 270 and 605 °C was observed to begin at so-called stage V recovery temperature (≈600 °C) and was completed at 980 and 1100 °C, respectively. Isothermal annealing performed at 700 °C indicated that the activation energy for recovery was 4.07–4.88 ± 0.83 eV, which is comparable to values for molybdenum self-diffusion [6].

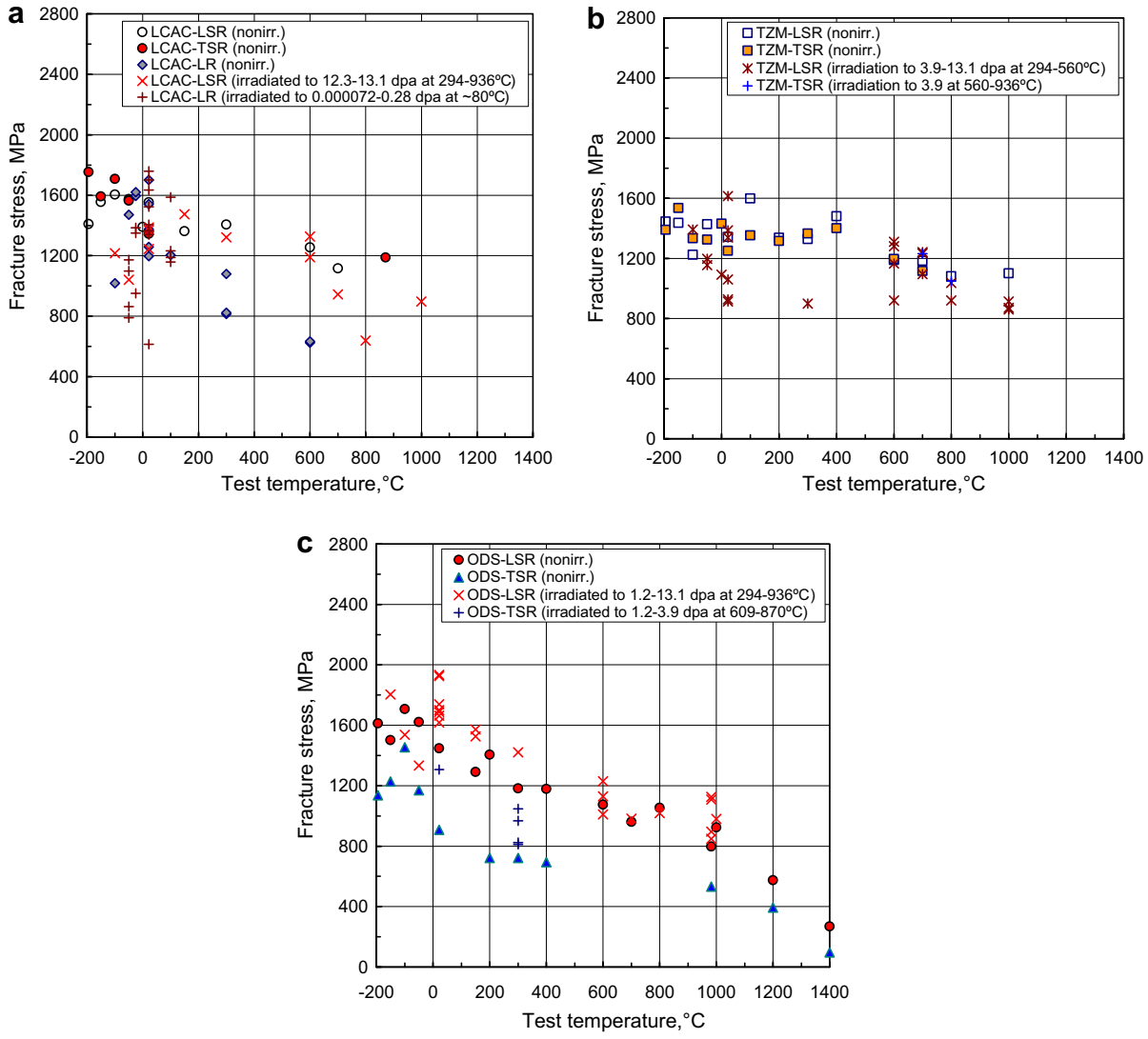

Fig. 3. Temperature dependence of the true fracture stress before irradiation for (a) LCAC molybdenum, (b) TZM alloy, and (c) ODS Mo.

These results indicate that the recovery of molybdenum irradiated at temperatures $\geqslant$605 °C occurs by the solid-state diffusion of vacancies to coarsen the dislocation loops and voids. Considering that the irradiation at 605 °C or around the stage V recovery temperature should result in an incomplete recovery, ~700 °C seems to be a lowest irradiation temperature for minimal irradiation hardening in these molybdenum materials.

3.2. Plastic instability stress

In uniaxial tensile deformation the metallic materials usually fail either by a localized necking (or a concentrated shear) process or by a brittle fracture before the shear process. The brittle fracture of irradiated metals generally results from an increase in the flow stress above the stresses for crack propagation. In ductile deformation the onset of unstable plastic deformation is considered the initiation of failure. Considére's criterion states that the plastic instability initiates when strain-hardening rate is equal to true stress, or at peak load, and is used to determine the critical stress and strain for the plastic instability [30]. Irradiation hardening is often accompanied by prompt initiation of necking. The dose dependence of the stress criterion for initiation of necking has been extensively studied for a few dozen materials [30], where it was confirmed that the stress criterion, or plastic instability stress (PIS), was dose independent. It was also found that the criterion could be applied to the materials hardened by other defects such as dislocation tangles produced by pre-strain [39]. Such defect independence was observed at all temperatures; which suggests that the test temperature dependence of PIS may not be affected by low-temperature irradiation. Note that PIS is defined only for the cases showing ductile deformation; the PIS value was not determined when brittle failure was observed so that the plastic yield stress was not measured.

Fig. 2 presents the test temperature dependence of PIS for nonirradiated and irradiated molybdenum materials (note that PIS cannot be calculated for the cases of low uniform ductility (<0.5%) and therefore is not presented for such cases). Fig. 2 indicates that overall temperature dependence of PIS resembles that of the yield stress of nonirradiated materials. The decreasing rate of PIS with temperature is high in the temperature range <200 °C; it becomes much lower at higher temperatures between ~200 and ~1000 °C, which is followed by an additional drop in the temperature range of 1000–1200 °C. Comparing the materials, the highest PIS values are found in TZM alloy over entire test temperature range. Again, the LCAC-LR material shows lowest PIS among the Mo materials. As predicted above, no evident radiation effect is found in the PIS data at any test temperature. This means that the plastic instability criterion remains the same after irradiation [30–32].

3.3. Fracture stress

Fig. 3(a) and (b) compare the true fracture stresses (FS) of LCAC molybdenum and TZM alloy before and after irradiation. It is observed that the FS has small negative slope to test temperature. In all cases the fracture stress data presents large scatter; this scatter tends to increase as the test temperature decreases. No FS less than ~600 MPa is found over the large temperature range (<~1000 °C), making ~600 MPa a lower bound. It is noted that some low fracture stresses, those <~1000 MPa at 300 °C or below and those <~700 MPa at higher temperatures, results from brittle fracture or localized shear failure only without diffuse necking. Further, as mentioned above, at −100 °C or below some specimens show reduced FS due to brittle failure. Comparing the FS data for nonirradiated and irradiated materials, a radiation induced decrease is obvious in some materials like LCAC-LR and TZM-LSR, but only at relatively low-temperatures. Also, except for the LCAC-LR material, no significant difference in FS is observed among the molybdenum materials; which indicates that the difference between specimen orientations (LSR and TSR) is not significant.

The FS data for the wrought ODS Mo are presented in Fig. 3(c). Overall, the ODS-LSR has the highest FS among the test materials, while those for ODS-TSR are similar to those of the other materials at low-temperatures and tends to be lower at elevated temperatures. The temperature dependence of FS for ODS Mo is similar to that of the other materials presented in Fig. 3(a). However, the effect of specimen direction is obvious, due to the fine and heavily elongated oxide particles and grain structure [3,7]. Over the entire test temperature range the fracture stresses of LSR specimens are 100–200 MPa higher than those of TSR specimens; which persists in both irradiated and nonirradiated conditions. While other strength data (i.e., YS and PIS for ODS alloy) display no significant difference from the data for the other stress-relieved molybdenum materials, one noticeable feature of this material is that the fracture stress increases after irradiation for both specimen directions (LSR and TSR). This may lead to a delay of embrittlement by irradiation and higher fracture toughness.

3.4. Tensile failure mode and transition temperature

It is attempted here to determine a critical temperature for the change of fracture mode by comparing the plots of stress versus temperature curves. The final fracture of a ductile material is always preceded by a subsequent process of diffuse and localized necking deformation. In molybdenum materials the onset of localized necking or concentrated shearing after diffuse necking prompts the final fracture, and therefore the fracture strength data measured at the end of tensile curves should be nearly identical with the axial strength for shearing in necking deformation. Further, it has been shown for a few dozen ductile alloys that the tensile FS in ductile failure has a strong relationship with the PIS [31,32], i.e.,

$$\mathrm{FS} \approx 2\mathrm{PIS} \tag{4}$$

Note that this equation with a coefficient of about 2 is valid for most body centered cubic (bcc) and hexagonal close packed (hcp) metals, but not for some soft pure bcc and most face centered cubic (fcc) metals. Fracture mode should be brittle or at least partially brittle if a specimen does not experience the localized necking before the

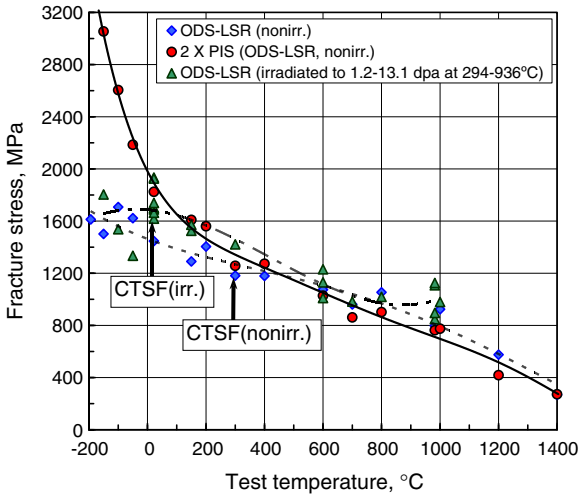

Fig. 4. Determination of the critical temperature for shear failure (CTSF) in ODS alloy.

Table 3
Critical temperature for shear failure (CTSF) and DBTT in tensile ductility

Material	Direction/heat treatment	CTSF (°C) before irradiation	CTSF (°C) after irradiation	DBTT (°C) before irradiation	DBTT (°C) after irradiation at ~300 °C	DBTT (°C) after irradiation at ~600 °C	DBTT (°C) after irradiation at >800 °C
LCAC	LSR	25	150	−100	800	300	−50
	TSR	~200		−100			<25
	LR	−25	25	−50			
TZM	LSR	100	600	−50	800	700	−50
	TSR	300	<700	−50		700	<0
ODS	LSR	300	25	−100	800	25	−100
	TSR	~900	~900	25		>25	<300

Note: LSR – longitudinal, stress-relieved; TSR – transverse, stress-relieved; LR – longitudinal, recrystallized. DBTTs, except for the value of LCAC-LR, were determined in earlier studies [5,7] using data for reduction in area.

final fracture or if it fractures before true stress reaches two times the PIS. In such a case, the measured FS versus temperature curve should show a significant deviation from the predicted curve which is given by 2 × PIS. It is believed therefore that the transition from ductile to non-ductile fracture modes after irradiation can be determined by comparing the true stress versus temperature curves for the nonirradiated material.

Fig. 4, for an example, compares the FS versus test temperature curves with the curve of 2 × PIS for the ODS Mo alloy. Two arrows indicate the critical temperatures at which the curves start to show deviations from the 2PIS line. The critical temperature is based on true stress parameters only and is named the critical temperature for shear failure (CTSF); above which (but below the temperature of thermal creep) the tensile failure should occur in ductile mode by a sequence of diffuse necking, localized necking (shear), and final fracture; below which the failure should occur in an partially or totally embrittled manner. Graphical determination of CTSF was processed for all test materials and the CTSF data are listed in Table 3, which also includes the ductile to brittle transition temperatures (DBTT) data determined from the temperature transition curves of the reduction of area in fractography [5,7].

Before irradiation, the ODS alloy has the highest CTSF and the LCAC Mo has a relatively low CTSF. In both the LCAC Mo and the TZM alloy the CTSF value increased after irradiation. It is noted that the increase of CTSF by irradiation is very large for the TZM alloy (i.e., 500 °C for TZM-LSR) while it is reduced or retained at similar value in ODS alloy. It is notable that a significant decrease of CTSF, 275 °C, is observed in ODS-LSR. Although the ODS-TSR specimens show highest CTSF among the materials and process conditions, a proper structural design associated with stress distribution should be able to avoid maximum tensile stress occurring in the transverse direction and the maximize the benefits from the low CTSF in the longitudinal direction. Although the DBTT measurements seem to be not closely related to CTSF because it is a strain-based parameter, key trends in the DBTT are generally similar to those of CTSF; a low CTSF in ODS-LSR and a large increase of CTSF in TZM alloy are reflected in the behavior of DBTT in a similar manner. Considering these transition temperatures, it is predicted that the ODS Mo specimens in the LSR condition may display the best fracture toughness among the test materials and conditions. The result on CTSF, which has a weak dependence on irradiation condition, also indicates that the dependence of fracture toughness on irradiation temperature will not be substantial after irradiation hardening is saturated at the irradiation temperature.

It is worth noting that tensile specimen can fail in a brittle mode above CTSF after low-temperature irradiation. The LCAC-LSR specimen irradiated at 300 °C to 12.3 dpa and tested at 600 °C is such a case: the specimen broke in a brittle mode at 1191 MPa, which is higher than the 2 × PIS value (PIS = 521 MPa). The specimen should break with limited plasticity whenever irradiation increases yield stress above 2 × PIS. Since the condition for the initiation of shear failure, 2 × PIS, is satisfied, the specimen is considered to fail in a brittle mode but the failure should be initiated by a localized shear. This is confirmed by the angled fracture surfaces, which differs from the true brittle failure cases with 90° between the loading direction and the fracture surface occurring at a fracture stress <2 × PIS at low-temperatures.

3.5. Effect of grain refinement

The high radiation resistance of ODS molybdenum in LSR condition is believed to result from its unique fine grain microstructure [3,7]. Although both the TZM alloy and the ODS Mo are dispersion hardened materials, the thermal stability and number density of lanthanum oxide particles in ODS Mo are believed to be higher at processing temperatures, and therefore the oxide particles can effectively prevent grain growth. As a result, a fine, highly elongated grain structure has been produced in the ODS Mo, as indicated in Fig. 5 [7]. It is also noted that all materials in stress-relieved condition (LSR and TSR) have highly elongated grains with aspect ratios ranging from 13 to 70. This elongated grain structure often exhibits laminated failure features [3,7]. Both grain diameter and grain length of ODS Mo are smallest among the stress-relieved materials. Cockeram et al. [7] have attributed the benefits to a sheet like fine grain structure; a high plasticity can be imposed to the grain structure by reducing the size of ductile laminate features formed in fracture process so that a plain strain condition is induced on each plane of the laminate-shaped grains. More defect sinks or boundaries are formed by refining the grains, which possibly reduces the number density of defect clusters such as dislocation loops and voids. This explanation also suggests that irradiation

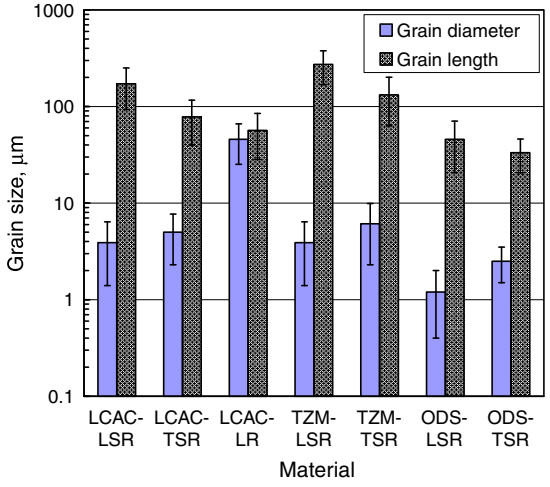

Fig. 5. Comparison of grain diameters and lengths for molybdenum materials.

hardening in ODS Mo will not be more significant than in other materials due to the reduced defect cluster formation, and that final fracture will be delayed by higher plasticity accumulation at laminate features. This agrees with the present analysis result that the increase of YS is similar for all three stress-relieved materials, while the fracture stress of ODS Mo in LSR condition is the highest.

Although plentiful defect sinks are believed to be responsible for much of the good resistance to irradiation embrittlement found in ODS Mo, the defect sink theory can not explain the increase of FS and decrease of CTSF because more defect sinks can only delay the embrittlement. Additional mechanisms responsible for such an increase of radiation resistance may be (a) stress-relief during irradiation and (b) redistribution of chemical elements at grain boundaries. Since there can still exist significant residual stress in the wrought ODS Mo structure after the typical stress-relief treatment at 1200 °C for 1 h, the irradiation at a high temperature may cause additional stress-relief and consequently ductilize further the material. Irradiation also may be able to knock out some atoms from oxide particles and modify the chemistry at grain boundaries. This can result in strengthening the boundaries and increase of fracture stress. Further study is needed to elucidate such mechanisms.

4. Conclusion

Radiation effects on mechanical properties were investigated for select molybdenum materials: LCAC Mo, TZM alloy, and ODS Mo. Comparisons for these materials were made by using the test temperature dependence of true stress parameters. The following conclusions were reached:

(1) The yield stress was strongly dependent on test temperature. Irradiation at relatively low-temperatures (<700 °C) increased the yield stress significantly while the increase of yield stress after irradiation at higher temperatures was minimal.
(2) The plastic instability stress was strongly dependent on test temperature but nearly independent of irradiation dose and temperature. The true fracture stress was less strongly dependent on test temperature, while irradiation at high temperatures did not significantly change the fracture stress.
(3) The critical temperature for shear fracture (CTSF) was defined and evaluated for the test materials based on the test temperature dependence of true stress parameters, and the CTSF values were compared with the ductile to brittle transition temperatures (DBTT).
(4) The ODS-LSR specimens showed the highest resistance to irradiation embrittlement due to relatively high fracture stress and low sensitivity to radiation. The increase of fracture stress lead to a decrease of CTSF in ODS-LSR material after irradiation.

Acknowledgement

This research was sponsored by the US Department of Energy, Office of Fusion Energy Sciences under Contract DE-AC05-00OR22725 with UT-Battelle, LLC. The authors express special thanks to Drs D. McClintock and C.E. Duty for technical reviews and comments.

References

[1] F.W. Wiffen, in: R.H. Cooper, E.E. Hoffman (Eds.), Technical Information Center (USDOE), Oak Ridge, Tennessee, 1984, p. 252.
[2] Y. Nemoto, A. Hasegawa, M. Satou, K. Abe, Y. Hiraoka, J. Nucl. Mater. 324 (2004) 62.
[3] B.V. Cockeram, Metall. Mater. Trans. A 33A (2002) 3685.
[4] B.V. Cockeram, J.L. Hollenbeck, L.L. Snead, J. Nucl. Mater. 324 (2004) 77.
[5] B.V. Cockeram, R.W. Smith, L.L. Snead, J. Nucl. Mater. 346 (2005) 145.
[6] B.V. Cockeram, J.L. Hollenbeck, L.L. Snead, J. Nucl. Mater. 336 (2005) 299.
[7] B.V. Cockeram, R.W. Smith, L.L. Snead, J. Nucl. Mater. 346 (2005) 165.
[8] S.K. Das, M. Kaminsky, P. Dusza, J. Vac. Sci. Technol. 15 (1978) 710.
[9] G.R. Smolik, D.A. Petti, S.T. Schuetz, J. Nucl. Mater. 283–287 (2000) 1458.
[10] Y. Kitsunai, H. Kurishita, M. Narui, H. Kayano, Y. Hiraoka, J. Nucl. Mater. 239 (1996) 253.
[11] S.A. Fabritsiev, A.S. Pokrovsky, J. Nucl. Mater. 152 (1998) 216.
[12] Y. Kitsunai, H. Kurishita, T. Kuwabara, M. Narui, M. Hasegawa, T. Takida, K. Takebe, J. Nucl. Mater. 346 (2005) 233.
[13] B.V. Cockeram, J.D. Ballard, E.K. Ohriner, T.S. Byun, M.K. Miller, L.L. Snead, J. Nucl. Mater. (submitted for publication).
[14] L. Northcott, Metallurgy of the Rarer Metals – 5. Molybdenum, Academic Press Inc., New York, 1956.
[15] J. Wadsworth, C.M. Packer, W.C. Coons, in: K.H. Miska, M. Semchyshen, E.P. Whelan, D.J. Kruzich (Eds.), AMAX Materials Research Center, 1985, p.13.
[16] R. Eck, J. Tinzl, in: K.H. Miska, M. Semchyshen, E.P. Whelan, D.J. Kruzich (Eds.), AMAX Materials Research Center, 1985, p. 21.
[17] M. Egan, T. Cookson, W. Schimmel, in: K.H. Miska, M. Semchyshen, E.P. Whelan, D.J. Kruzich (Eds.), AMAX Materials Research Center, 1985, p. 33.
[18] H. Kurishita, H. Yoshinaga, in: K.H. Miska, M. Semchyshen, E.P. Whelan, D.J. Kruzich (Eds.), AMAX Materials Research Center, 1985, p. 87.
[19] A.J. Bryhan, in: K.H. Miska, M. Semchyshen, E.P. Whelan, D.J. Kruzich (Eds.), AMAX Materials Research Center, 1985, p. 91.
[20] A.J. Bryhan, Joining of Molybdenum Base Metals and Factors Which Influence Ductility, Welding Research Council Bulletin, Bulletin 312, New York, February 1986, ISSN 0043-2326.
[21] M.K. Miller, E.A. Kenik, M.S. Mousa, K.F. Russell, A.J. Bryhan, Scr. Mater. 46 (2002) 299.
[22] M.K. Miller, A.J. Bryhan, Mater. Sci. Eng. A 327 (2002) 80.
[23] M. Tanaka, K. Fukaya, K. Shiraishi, Trans. JIM 20 (1979) 697.
[24] N.N. Morgunova, L.N. Demina, N.I. Kazakova, Met. Sci. Heat Treat. (USSR) 28 (1986) 895.
[25] V.V. Bukhanovskii, N.G. Kartyshov, E.G. Polishchuk, V.K. Kharchenko, M.I. Chikunov, Strength Mater. (USSR) 19 (1987) 1093.
[26] F. Lee, J. Moteff, in: K.H. Miska, M. Semchyshen, E.P. Whelan, D.J. Kruzich (Eds.), AMAX Materials Research Center, 1985, p. 147.
[27] M. Li, N. Hashimoto, T.S. Byun, L.L. Snead, S.J. Zinkle, J. Nucl. Mater. 367–370 (2007) 817.
[28] M. Li, N. Hashimoto, T.S. Byun, L.L. Snead, S.J. Zinkle, J. Nucl. Mater. 371 (2007) 53.
[29] M. Li, M. Eldrup, T.S. Byun, N. Hashimoto, L.L. Snead, S.J. Zinkle, Low temperature neutron irradiation effects on microstructure and tensile properties of molybdenum, J. Nucl. Mater. 376 (1) (2008) 11.
[30] T.S. Byun, K. Farrell, Acta Mater. 52 (2004) 1597.
[31] T.S. Byun, N. Hashimoto, K. Farrell, J. Nucl. Mater. 303 (2005) 351.
[32] T.S. Byun, J. Nucl. Mater. 361 (2007) 239.
[33] L.K. Keys, J.P. Smith, J. Moteff, Phys. Rev. Lett. 22 (1969) 57.
[34] L.K. Keys, J. Moteff, J. Appl. Phys. 41 (1970) 2618.
[35] M.I. Zakharova, V.A. Solov'ev, V.N. Bykov, Atom. Energy 38 (1975) 101 (Translated from Atomnaya Energiya 30 (2) (1975) 78).
[36] H.I. Jang, J. Moteff, in: Properties of Reactor Structural Alloys after Neutron or Particle Irradiation, ASTM STP 570, American Society for Testing Materials Philadelphia, PA, 1975, p. 404.
[37] S. Mantl, W. Triftshäuser, Phys. Rev. B 17 (1978) 1645.
[38] M. Eldrup, B.N. Singh, S.J. Zinkle, T.S. Byun, K. Farrell, J. Nucl. Mater. 301 (2002) 912.
[39] T.S. Byun, K. Farrell, Acta Mater. 52 (2004) 3889.